Direct atomistic observation of deformation in multiwalled carbon nanotubes

Tokushi Kizuka*
Department of Applied Physics, School of Engineering, and Research Center for Advanced Waste and Emission Management, Nagoya University, and PRESTO, JST, Furo-cho, Chikusa-ku, Nagoya, 464-8603, Japan
(Received 26 June 1998)

The deformation process of individual multiwalled carbon nanotubes was directly observed by time-resolved high-resolution transmission electron microscopy using a piezo-driving specimen holder at a spatial resolution of 0.2 nm and a time resolution of 1/60 s. High elasticity and the subsequent atomistic damage process of the nanotubes were demonstrated. [S0163-1829(99)13503-3]

Since the discovery of the carbon nanotube as a structure,[1] its mechanical properties have been investigated for technological applications to elements of nanometer-structured composites or electronic devices. The high flexibility of the nanotubes was shown by atomic force microscopy (AFM).[2] Young's modulus in the terapascal range was also measured based on observations of small thermal vibration of the isolated nanotubes.[3] However, other kinds of fundamental mechanical properties, such as the elastic limit, plasticity, and fatigue, are still unknown. The atomistic structural dynamics during deformation has been studied in relation to this problem. The deformation process was simulated using molecular dynamics,[4,5] and the bending structures were observed after the deformation by static high-resolution transmission electron microscopy (HRTEM).[6–8] The present time-resolved HRTEM at a spatial resolution of 0.2 nm and a time resolution of 1/60 s using a piezodriving specimen holder[9,10] enables us to make direct atomistic observations of the deformation process of individual nanotubes. High elasticity and the subsequent atomistic damage process are demonstrated in this study.

Multiwalled carbon nanotubes were obtained by arc discharge using two graphite carbon electrodes in argon at 1.3 $\times 10^4$ Pa. The specimens were aggregates of carbon nanotubes and onion-structured fullerenes. The aggregates were fixed on the specimen mounts of the mobile and fixed sides

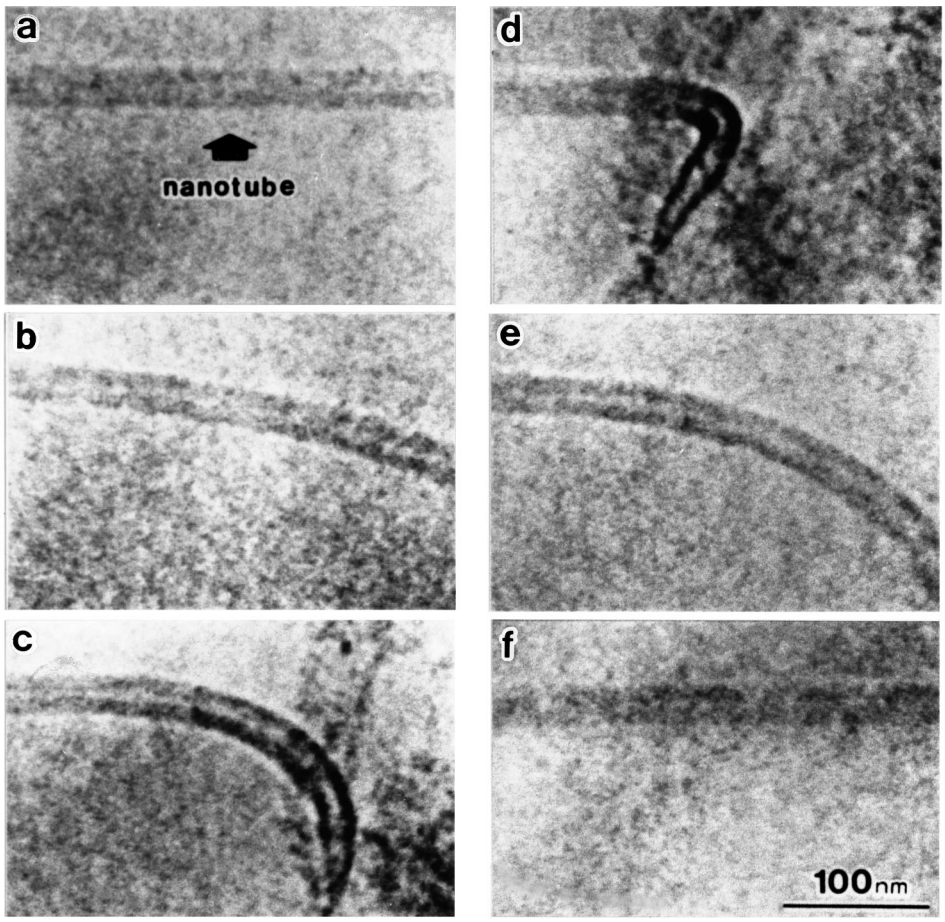

FIG. 1. Time-sequence series of bright-field images of the elastic deformation process of a carbon nanotube. The time interval of the images is 6 s.

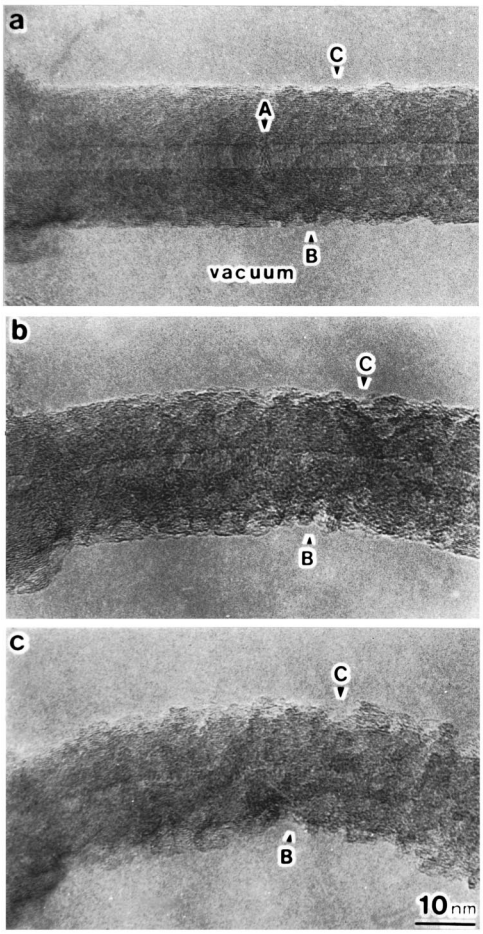

FIG. 2. Time-sequence series of high-resolution images othe fatigue process of a carbon nanotube after several repeated elastic deformations. The time interval of the images is 6 min. The images were recorded after stress relief. Relatively lower magnification images are shown in the upper column. Arrow *A* shows an inner wall. Enlarged images of the compressive and tensile regions indicated by arrows *B* and *C* in the upper column are shown in the lower left and right columns, respectively. The bending angles are 0° (a), 21° (b), and 31° (c).

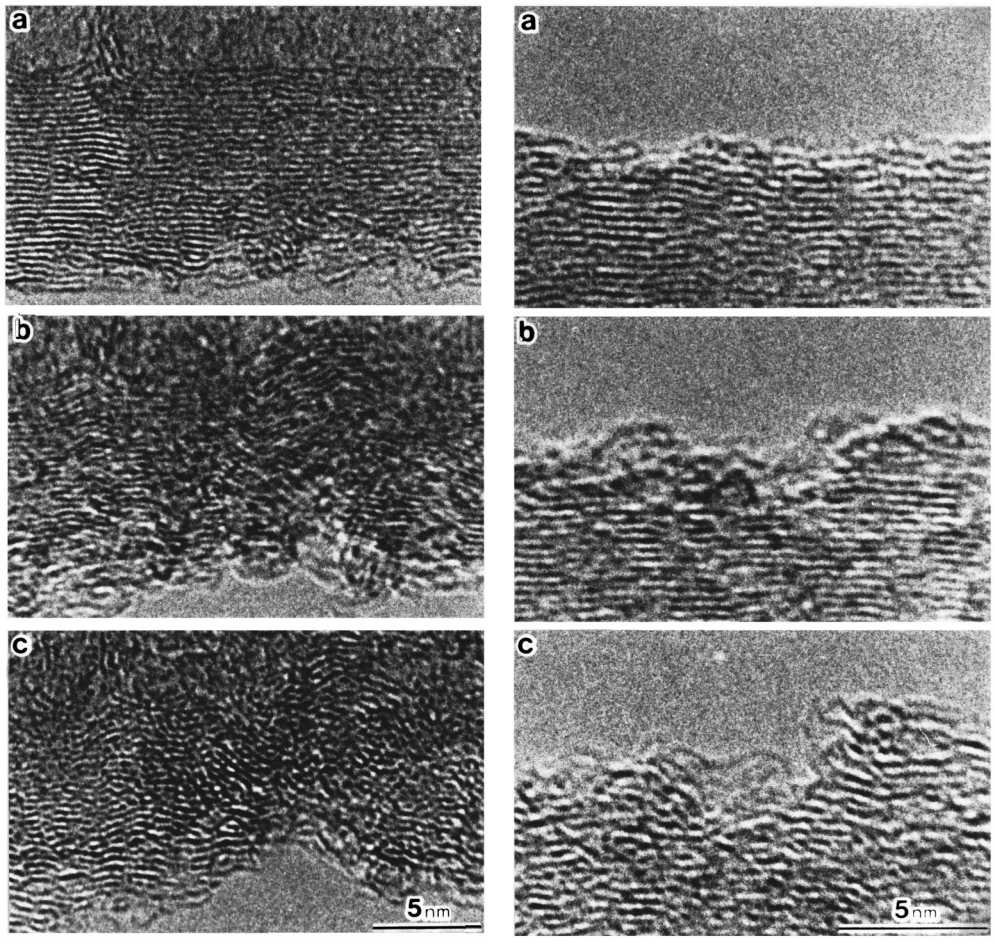

of the piezodriving specimen holder[9,10] for the atomic scale mechanical tests. A carbon nanotube, which protruded from the aggregate on the fixed side, was compressed at room temperature by piezodriving using the tip on the mobile side in a 200-kV high-resolution transmission electron microscope equipped with a LaB_6 thermionic gun (JEOL: JEM-2010). Time-resolved HRTEM observations were simultaneously carried out. A silicon integrated target television camera (LHESA: LH-4036) and a S-VHS-type video tape recorder with two digital frame memories were employed for the dynamic observations in addition to a conventional film-recording system. The time-sequential images recorded on video tape in this work were obtained by averaging four video frames using a digital frame image-processing system (Japan Avionics: Image Sigma). The time resolution of the present system was 1/60 s, corresponding to the time for half of a frame (one field) of the image in the NTSC TV system. The electron-beam irradiation density ranges from 1 to 30 $\times 10^4$ A/m^2. The pressure around the specimen in the electron microscope was around 2×10^{-5} Pa. The spherical aberration constant of the objective lens in the microscope was 0.5 mm, and the point-to-point resolution at 200 kV was 0.19 nm.

Figure 1 shows a time sequence series of bright-field images for the deformation process in a carbon nanotube. The internal and external diameters and length of the nanotube are 5, 28, and 660 nm, respectively. First, the external shape of the nanotube is straight [Fig. 1(a)]. The tip of the nanotube on the fixed side contacts with the processing tip of the carbon aggregate on the mobile side. The processing tip is subsequently displaced along the same direction, and the stress is applied to the nanotube resulting in it being bent at an angle of more than 90° [Figs. 1(b)–1(d)]. The initial buckling force was calculated later. The processing tip is then displaced along the opposite direction [Fig. 1(e)]. The external shape of the nanotube recovers after the stress is relieved [Fig. 1(f)]. The process of stress loading and relieving was repeated a few times and the external shape recovered. This observation shows clearly that the nanotube deforms elastically up to a high bending angle of over 90°.

After such repeated deformations, the nanotubes did not recover, even though they were bent within the elastic limit; fatigue occurs during the elastic deformation. Figure 2 shows a time-sequence series of high-resolution images of the fatigue process of a carbon nanotube. The internal and external diameters and length of the nanotube are 4, 27, and 300 nm, respectively. The number of walls is 32. The atomic layers of the nanotube are distorted due to the repeated elastic deformation though its external shape is straight [Fig. 2(a)]. The processing tip is displaced through the same process as the repeated elastic deformation; similar stress is applied and relieved. The nanotube remains bent after the stress is relieved [Fig. 2(b)]. The atomic layers on the compressive side are wavy while those on the tensile side are beginning to break. In particular, a larger localized depression occurs on the compressive side as indicated by arrow *B* in Fig. 2(b) beside a small inner wall [Fig. 2(a), arrow *A*]. This shows that the inner wall contributes to the increase in bending strength. At the outer side of the depression, a larger breakage occurs [Fig. 2(b), arrow *C*]. The depression on the compressive side and the breakage on the tensile side become larger after the stress loading and relieving is repeated once again [Fig. 2(c)]. The columnar void along the central axis is collapsed at the depression. The bending angle in Fig. 2(c) is larger by 10° than that in Fig. 2(b).

The applying force at the initial stage in the present deformation, i.e., Euler's bucking force P_{Euler} is estimated using the formula[11]

$$P_{\mathrm{Euler}}=\pi^2 EI/l^2,$$

where E is Young's modulus, I is the stress moment over the cross section of the nanotube, and l is the length of the nanotube. E was measured to be from 0.40 to 3.11 TPa for the nanotubes of various lengths and diameters.[3] In their measurements, the shape of a nanotube of 6.6 nm in inner diameter, 24 nm in external diameter, and 5.8 μm in length is similar to those of the present nanotubes. E was 0.59 TPa for the nanotube. We selected $E=0.59$ TPa for the similarity in the shape. I is expressed as

$$I=\pi(d_2^4-d_1^4)/64,$$

where d_1 and d_2 are the internal and external diameters of the nanotube, respectively. I is 3.0×10^{-32} and 2.6×10^{-32} m^4 for the nanotubes in Figs. 1 and 2, respectively. As a result, P_{Euler} is estimated to be 4×10^{-7} N for the nanotube in Fig. 1 and 2×10^{-6} N for the nanotube in Fig. 2.

For comparison, we estimate P_{Euler} for graphite whiskers. E was measured to be 0.7 TPa.[12] P_{Euler} for the whisker is 2×10^{-6} N when the shape is the same as that of the nanotube in Fig. 2. Thus both values of P_{Euler} are in the same order.

In conclusion, it was found that (1) nanotubes can be bent elastically up to a high angle; and (2) the fatigue of a nanotube occurs due to the distortion of atomic layers in the entire region, the waving and depressions of the layers on the compressive side, and the breakage of the layers on the tensile side. The high elasticity can be harnessed for use in scanning tips of AFM and elements of nanometer-structured materials.

The author would like to thank Kaori Hirahara, a graduate of Nagoya University, for help with photograph preparation, and Mikio Naruse and Shunji Deguchi of JEOL Ltd. for cooperation in developing the piezodriving specimen holder. Financial support was provided for the present study by TEPCO Research Foundation, Kawasaki Steel 21st Century Foundation, and the Sumitomo Foundation. The present study was partly supported by a Grant-In-Aid from the Japanese Ministry of Education, Science and Culture.

*FAX: 81-52-789-4458. Electronic address: j46110a@nucc.cc.nagoya-u.ac.jp

[1] S. Iijima, Nature (London) **35**, 56 (1991).

[2] M. R. Falvo, M. G. J. Clary, R. M. Taylor, V. Chi, F. P. Brooks, Jr., S. Washburn, and R. Superfine, Nature (London) **389**, 582 (1997).

[3] M. M. J. Treacy, T. W. Ebbesen, and J. M. Gibson, Nature (London) **381**, 678 (1998).

[4] B. I. Yakobson, and R. E. Smalley, Am. Sci. **85**, 324 (1997).
[5] C. F. Cornwell, and L. T. Wille, Solid State Commun. **101**, 555 (1997).
[6] S. Iijima, J. Chem. Phys. **104**, 2089 (1996).
[7] Y. Ishida, T. Kuzumaki, T. Hayashi, and K. Ito, Mater. Sci. Forum **207-209**, 161 (1996).
[8] D. N. Weldon, W. J. Blau, and H. W. Zandbergen, Chem. Phys. Lett. **241**, 365 (1995).
[9] T. Kizuka, K. Yamada, S. Deguchi, and M. Naruse, Phys. Rev. B **55**, R7398 (1997).
[10] T. Kizuka, K. Yamada, S. Deguchi, and M. Naruse, J. Electron Microsc. **46**, 151 (1997).
[11] H. Dai, J. H. Hafner, A. G. Rinzler, D. T. Colbert, and R. E. Smalley, Nature (London) **384**, 147 (1996).
[12] R. Bacon, J. Appl. Phys. **31**, 283 (1960).